data

Data Descriptor

A Dataset of Annotated DICOM Images of Head CT Angiography for Intracranial Aneurysm Detection

Evgenia Blagosklonova [1], Daria Dolotova [1,2,*], Natalia Polunina [3,4], Elena Grigorieva [5], Denis Pakhomov [1], Vladimir Krylov [3,4] and Andrey Gavrilov [1,6]

[1] Gammamed-Soft, Ltd., 127473 Moscow, Russia; evgenia.blagosklonova@gammamed.ru (E.B.); denis.pakhomov@gammamed.ru (D.P.); andrey.gavrilov@gammamed.ru (A.G.)
[2] Research and Clinical Institute for Pediatrics Named after Yuri Veltischev, Pirogov Russian National Research Medical University, 125412 Moscow, Russia
[3] Department of Fundamental Neurosurgery, Pirogov Russian National Research Medical University, 117513 Moscow, Russia; polunina_na@rsmu.ru (N.P.); krylov_vv5@rsmu.ru (V.K.)
[4] Moscow Healthcare Department, N.V. Sklifosovsky Research Institute for Emergency Medicine, 129090 Moscow, Russia
[5] Clinical Medical Center, Ministry of Healthcare of Russia, Russian University of Medicine, 127006 Moscow, Russia; grigorieva_ev@rosunimed.ru
[6] Laboratory of Medical Computing System, Scobeltsyn Nuclear Physics Research Institute, Lomonosov Moscow State University, 119991 Moscow, Russia
* Correspondence: dolotova_dd@rsmu.ru; Tel.: +7-905-711-3769

Abstract

Rupture of Intracranial Aneurysms (IAs) is the leading cause of non-traumatic intracranial hemorrhage. Early detection of aneurysms prior to rupture or their prompt identification in cases of intracranial hemorrhage is critical and guides treatment strategies. The development of artificial intelligence tools to automate the labor-intensive detection and analysis of IAs is an active research field, but it depends on the availability of large, well-curated datasets for robust model training, validation, and testing. Collaborative data sharing is essential for advancing this field, yet remains relatively uncommon. Here, we present a collection of 172 Computed Tomography Angiography (CTA) scan series—a widely available and commonly used modality for the diagnosis of IAs—supplemented with structured metadata. The dataset comprises 90 scans from healthy patients and 82 scans from patients with IAs of diverse shapes, sizes, and anatomical locations, annotated and validated by two experts. The annotations include 122 surface mesh models in STL format. This openly accessible dataset is intended to support the development of automated segmentation or classification tools, medical image analysis, and assessment of disease progression risks through morphometric and hemodynamic evaluations.

Dataset: https://doi.org/10.5281/zenodo.15697196.

Dataset License: CC-BY 4.0

Keywords: intracranial aneurysm; computer tomography angiography; dataset; artificial neural networks; segmentation; annotation; training sample; aneurysm rupture; SAH

Academic Editor: Rüdiger Pryss

Received: 23 January 2026
Revised: 21 March 2026
Accepted: 25 March 2026
Published: 3 April 2026

1. Summary

An aneurysm is an outpouching of an arterial wall caused by structural abnormalities. Under continuous hemodynamic stress, the aneurysmal dilatation can progress and ultimately rupture, leading to hemorrhage. Intracranial Aneurysms (IAs) are particularly dangerous, as their rupture is the most common cause of non-traumatic intracranial hemorrhages [1]. Brain hemorrhages are associated with high mortality and disability rates, making early diagnosis and treatment crucial [2,3]. Timely detection of unruptured IAs is also critical for risk stratification and for selecting preventive management strategies, particularly as the rate of incidental—often asymptomatic—detections is rising with the expanding use of imaging.

Diagnosis, surveillance, and treatment planning for IAs are imaging-dependent and resource-intensive. Digital Subtraction Angiography (DSA) remains the reference standard, yet Computed Tomography Angiography (CTA) and Magnetic Resonance Angiography (MRA) are more widely used, owing to their noninvasive nature and broad availability [4]. Because of the considerable variability in IA shape, size, and location, accurate image interpretation demands thorough slice-by-slice review, as well as post-processing procedures such as multiplanar and three-dimensional (3D) reconstructions, and adjustment of density display, orientation, and slice thickness. Findings must also be differentiated from adjacent vessel fragments, contrast-related artifacts, and other vascular abnormalities. Rising imaging volumes, together with the labor-intensive nature of visual review, increase radiologists' workload and the risk of diagnostic error—especially when studies are performed for unrelated conditions; this risk also depends on reader experience and subspecialty, aneurysm size, and image quality.

Recent years have seen intense efforts to introduce machine-learning–based computer-aided diagnostic tools into clinical practice for segmenting anatomical structures and automatically detecting pathology on radiological images [5]. Using such tools to flag regions that require a physician's attention can substantially accelerate the diagnostic process and reduce errors—particularly relevant for IAs. The capabilities of these tools can be extended beyond aneurysm detection to the provision of additional diagnostically important information. For example, Feng et al. created a tool that automatically detects aneurysms, performs segmentation and morphological measurements, and also identified radiomic features that differentiate ruptured from asymptomatic aneurysms [6]. Xie et al. used deep learning and radiomics to identify aneurysms prone to rupture [7]. The training data play a pivotal role in achieving diagnostic performance. In addition to the obvious need for large case numbers and high-quality annotation, it is important that training sets encompass the full diversity of the target pathology. For clinical deployment, algorithms should be validated on representative multicenter datasets. In many existing publications, training datasets include only a few hundred studies, are typically limited to a single institution and scanner, and are tested without external data—factors that may impair the reproducibility of the resulting models [8–10]. Datasets are also often constructed for a specific clinical task and have limitations such as the absence of patients without the target pathology [10,11], inclusion of only ruptured or only asymptomatic aneurysms [11,12], or restriction to aneurysms of particular shapes and sizes [13]. These constraints may ultimately limit real-world clinical applicability of new algorithms and tools.

Beyond detecting pathology per se, radiological findings form the basis for decisions about surgical treatment and play an important role in investigating the pathophysiology of IA formation and progression. Assessing the rupture risk of a detected aneurysm remains an unresolved challenge. Existing scales such as PHASES (Population, Hypertension, Age, Size, Earlier Sah, Site) [14] and UIATS (Unruptured Intracranial Aneurysm Treatment Score) [15], which estimate the need for surgery based on key clinical and morphological factors, have not undergone large-scale prospective validation of their reliability [16], and in most cases physicians make decisions based on morphometric indicators. At the same time, numerous studies report a weak correlation between IA size and rupture and emphasize the need to account—on a per-case basis—for three-dimensional aneurysm parameters [17] and local hemodynamics features obtainable through computational modeling [18]. In many such studies, the sample size is small, and limited data is cited as a major limitation.

Given the well-known challenges of collecting medical data, information sharing among researchers could make a significant contribution to improving diagnosis and understanding IA pathogenesis, yet it remains difficult. Despite the importance of the problem, there is a shortage of publicly available IA datasets. At present, collections of Time-Of-Flight Magnetic Resonance Angiography (TOF-MRA) and 3D rotational angiography (3DRA) are most common, and in most cases, they include relatively small samples. A recently published dataset by de Nys et al. [19] contains annotated TOF-MRA studies from 63 patients with IA, including longitudinal follow-up for 24 of them, which is a valuable contribution to studying disease progression. However, it lacks data from healthy subjects. Another public TOF-MRA collection published by Di Noto et al. [20] includes annotated images from 157 patients with IA and 127 healthy controls. Neither dataset includes cases with ruptured IA. Additional downloadable datasets have been released as training sets for challenges on aneurysm detection and analysis: the "Cerebral Aneurysm Detection and Analysis Challenge (CADA)" [21], which provides 109 3DRA images from patients with IA, and the "Aneurysm Detection And segMentation Challenge (ADAM)" [22], which provides TOF-MRA from 113 patients, 93 of whom had IAs. From 2015 to 2020, the international AneuX project [23] collected 750 three-dimensional models of ruptured and unruptured aneurysms reconstructed from 3DRA. The dataset also incorporated earlier projects, @neurIST [24] and Aneurisk [25]. The AneuX database, like several other collections [26,27], does not contain raw images, which limits its applicability. Although CTA is the most common and accessible modality for visualizing the vasculature in medical institutions and offers non-invasive acquisition with rapid scanning and high spatial resolution [28], there is currently only one large open dataset containing CTA data. Bo et al. published an annotated multicenter CTA dataset from six institutions that includes 1338 image series, supplemented by an external dataset with 138 examinations from two institutions [29]. The dataset includes both ruptured and unruptured aneurysms larger than 2 mm, of various shapes and locations; however, data from healthy subjects are present only in the external set (96 cases). More recently, an open dataset including non-contrast Computed Tomography (CT) and CTA from 143 patients—99 of them with ruptured and unruptured aneurysms—was released [30]. That dataset includes only middle cerebral artery aneurysms but provides extensive additional information, including three-dimensional aneurysm models and aneurysm-with-parent-artery models, as well as rich clinical data.

It is therefore essential to expand open datasets to provide researchers with multicenter and multinational data for advancing tools that assist in interpreting medical images and for use in clinical decision-support systems. Data sharing is especially important for IAs because of the wide variability in location, extent of arterial involvement, and morphology. Classically, aneurysms are categorized by shape into saccular and non-saccular. Saccular aneurysms are lateral outpouchings of the arterial wall. Non-saccular aneurysms involve a segment of an artery (fusiform IAs) or a vascular bifurcation [31]. Aneurysms frequently display atypical morphology; they may have daughter sacs and can combine features of fusiform dilatation with a large lateral outpouching. Another recognized subtype is a blister-like aneurysm, typically broad-necked and shallow, with an aggressive clinical course [32]. These IAs are not amenable to standard surgical techniques and are classified as "complex". Additional complicating factors include difficult-to-reach locations, giant size, vessels arising from the aneurysm dome, thrombosis, and wall calcification [33,34]. Very small ("miliary") aneurysms up to 3 mm warrant additional attention; they are difficult to diagnose and are often not considered a potential cause of hemorrhage, yet ruptures of such aneurysms have been reported [35]. This diversity of morphological presentations complicates the study of IAs and their treatment when observations are limited.

This diversity of pathology and the uniqueness of each case complicate the study of IAs and their treatment when observations are limited.

In this study, we compiled a CTA dataset comprising contrast-enhanced head CT images from patients with and without IAs, together with expert aneurysm segmentations. The dataset is accompanied by patient-level metadata and a detailed IA classification scheme to facilitate reuse by researchers. It can be used to develop, test, and validate algorithms for automatic IA detection and classification; for segmentation of the intracranial arterial tree; for texture-analysis tasks; for analyses of aneurysm morphology; and for blood-flow simulations using physical and mathematical models. Three-dimensional models generated from CTA volumes may also support training and the planning of surgical or endovascular treatment, including device selection and placement [36].

A current limitation of the dataset is the absence of postoperative studies with implanted devices and cases involving neoplasms or arteriovenous malformations, which—given the differential diagnosis with IA—could significantly improve the performance of automatic detection algorithms. Another inherent limitation relates to the sampling strategy: while the non-IA group was formed by random sampling among patients who underwent CTA, IA cases were collected consecutively to capture the full spectrum of the pathology. Furthermore, despite our efforts to include diverse aneurysm morphologies, the sample size remains modest for certain rare subtypes, which may affect the statistical power of subtype-specific analyses.

Overall, this dataset represents a comprehensive collection of CTA head images, including both patients with and without intracranial aneurysms, accompanied by expert-annotated segmentations and detailed metadata. Its diverse and multicenter nature aims to facilitate the development of robust machine learning algorithms for aneurysm detection, classification, and morphological analysis. Although some limitations exist, the dataset offers a valuable resource for advancing diagnostic tools and supporting clinical decision-making in cerebrovascular disease. We hope it will contribute to filling the current gaps in publicly available neurovascular imaging data, fostering collaborative research and innovation.

2. Data Description

All data described in this article are available in the Zenodo repository [37] (https://doi.org/10.5281/zenodo.15697196) and occupy approximately 25.6 GBs of storage.

2.1. Dataset Composition

The root "Dataset" directory contains the metadata file, the "Studies" directory with tomographic examinations, and the "Annotations" directory containing segmented objects (Figure 1).

Each case is assigned a unique identifier used as the filenames in both study and segmentation folders. The file Metadata.csv contains a table listing the studies included in the dataset along with all accompanying information. The "Studies" directory contains subfolders with DICOM (Digital Imaging and Communications in Medicine) data; each subfolder is named according to the corresponding study identifier. The "Annotations" folder contains segmentation files of all intracranial aneurysms in STL format (.stl). Considering that some patients harbor multiple aneurysms, the IA segmentation filenames consist of the patient identifier and the object's sequential index as specified in the "IA" column of the table (not including the total number of aneurysms). The coordinates of all segmented objects are aligned with the coordinate system of the original images.

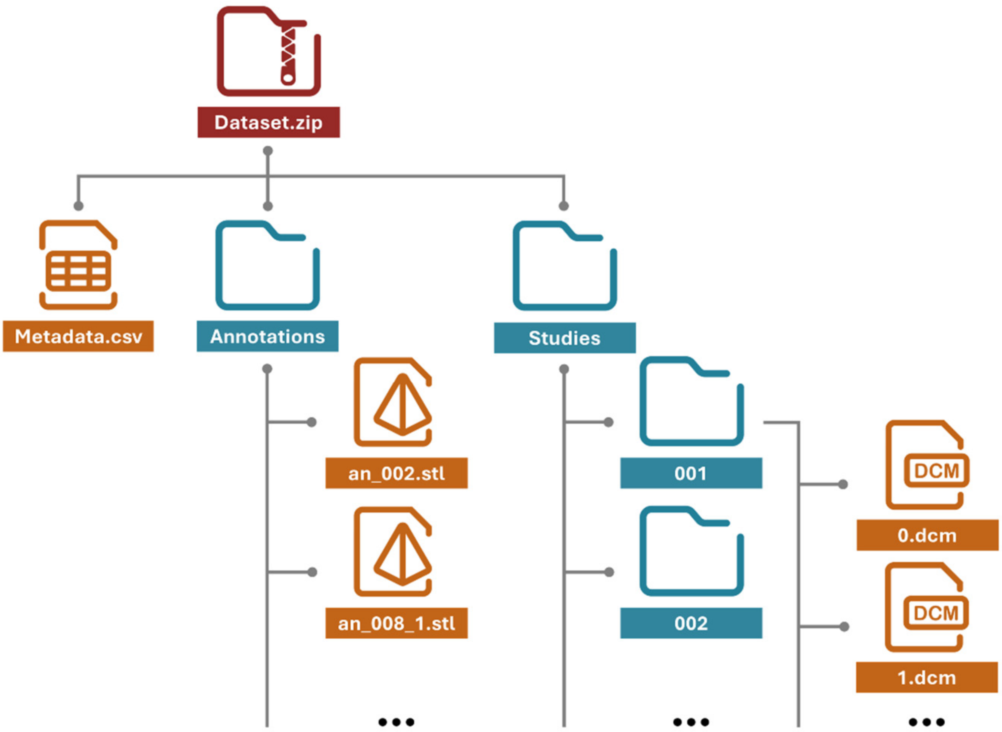

Figure 1. Folder structure of the dataset.

2.2. Metadata File Structure

The metadata file provides additional patient-level information and may be used for downstream analysis or for filtering according to predefined criteria. The data are stored as a table containing demographic information (including age and sex), the involved artery (including laterality), aneurysm rupture status, aneurysm classification and morphological parameters, as well as the number of slices, slice thickness, and whether the images extend inferiorly to include the neck (Table 1).

The value in the "IA" column consists of two numbers separated by an underscore: the first indicates the aneurysm's index number, and the second indicates the total number of aneurysms for that patient. Columns coded as "0/1" are binary and denote the presence or absence of the feature for the data entry. If a value was unavailable, "NA" was recorded.

Table 1. Components of the metadata table.

Characteristic Name	Description	Characteristic Format and Values
ID	Unique patient identifier	Number (1–N)
IA	Aneurysm Count	Number (0–i_N): 0—without aneurysm, i—aneurysm sequence number, N—total number of aneurysms in the case
Sex	Patient sex	F–female M–male
Age	Patient age, years	Number

Table 1. *Cont.*

Characteristic Name	Description	Characteristic Format and Values
Artery	Parent artery (if several arteries are affected by aneurysm, the proximal one is noted)	(L/R) ICA—left/right internal carotid artery (L/R) MCA—left/right middle cerebral artery (L/R) PCA—left/right posterior cerebral artery (L/R) ACA—left/right anterior cerebral artery BA—Basilar artery AComA—anterior communicating artery MACC—median artery of the corpus callosum
Saccular	Classification of aneurysm shape as saccular	0–non-saccular shape 1–saccular shape
Position	Aneurysm position classification relative to the parent artery	lateral bifurcation NA (unclassifiable, not applicable for this case)
Type	Extended aneurysm classification by shape	blister-like fusiform eccentric-fusiform fusiform-saccular NA (unclassifiable, not applicable for this case)
Size	Aneurysm classification by maximum size	miliary (<3 mm) middle (3–15 mm) large (15–25 mm) giant (≥25 mm)
Neck	Neck size (as available), mm	Number
Length	Aneurysm maximum length, mm	Number
Width	Aneurysm maximum width, mm	Number
Volume	Aneurysm volume, mm^3	Number
Rupture	Aneurysm rupture event	0–no rupture event 1–rupture with hemorrhage
Bleb	Aneurysm wall secondary bulge	0–no blebs 1–bleb present
Thrombus	Thrombosed aneurysm	0–no thrombus 1–thrombus present
Vessel	Vessel arising from the aneurysm	0–no vessel arising from the aneurysm 1–presence of vessel
Calcification	Aneurysm wall calcification	0–no calcification 1–presence of calcification
Images Count	Total number of image (slices) in series	Number
Slice Thickness	DICOM image slice thickness, mm	Number
Head + Neck	The examination includes the carotid bifurcation area	0–only head in the scanning area 1–head and neck within the scanning area

3. Methods

3.1. Data Collection

The study was conducted across three healthcare institutions: the N.V. Sklifosovsky Research Institute for Emergency Medicine (lead institution), the Clinical Medical Center of the Russian University of Medicine, and the Moscow Multidisciplinary Clinical Center "Kommunarka" of the Moscow Healthcare Department. The study was conducted in accordance with the Declaration of Helsinki, and approved by the Biomedical Ethics Committee of the N.V. Sklifosovsky Research Institute for Emergency Medicine (Protocol No. 2-23 dated 28 March 2023). Since the institutions provided access to pre-anonymized retrospective data, no informed consent was required.

Data were collected using consecutive sampling. All patients diagnosed with IAs, regardless of size, shape, or location, who were admitted to the neurology and neurosurgery departments between 2022 and 2023 were included. The IA-negative group was formed through random sampling among patients who underwent head CTA with a slice thickness of no more than 2 mm until the number of IA-negative cases approximately matched the number of IA cases.

In total, the final dataset comprised 172 cases: 82 (48%) with at least one IA (122 aneurysms in total) and 90 (52%) without aneurysms. Single aneurysms were present in 58 patients, while the remaining patients had multiple aneurysms (29% of IA patients). Additionally, nine patients had aneurysmal rupture confirmed by radiological and clinical evidence, with intracranial hemorrhage of varying severity (11% of patients with aneurysms). Patient ages ranged from 17 to 94 years (mean 60 ± 16 years), with 42% male and 58% female. Key population characteristics and aneurysm parameters are detailed in Tables 2 and 3.

Table 2. Demographic Data (n = 172).

Category (Characteristic)	Cases, *n* (%)
Sex, male	72 (42%)
Sex, female	100 (58%)
Age, years (M ± SD)	60 ± 16

Patients with severe atherosclerotic disease of the intracranial arteries, vascular malformations, oncologic disease, or a surgical history within the scanned region were not included. Examinations with artifacts that substantially distorted the region of interest or violated the scanning protocol—specifically, cases in which arterial opacification was insufficient to permit confident image interpretation—were also excluded. At the same time, examinations in which the presence of artifacts and suboptimal vascular opacification did not affect diagnostic confidence were retained. Owing to the profiles of the contributing departments, the IA-negative group included conditions such as arterial stenosis and occlusion, which improves the validity and scalability of algorithms developed using this dataset given the prevalence of these conditions.

All studies included in the dataset were evaluated by two specialists—a radiologist and a neurosurgeon, each with more than 20 years of experience—who also annotated the IA-positive cases.

Table 3. Aneurysm Characteristics (*n* = 122).

Category (Characteristic)	Description	Cases, *n* (%)
Aneurysms Count	0	90
	1	58 (71%)
	2	15 (18%)
	3	4 (5%)
	4	3 (4%)
	5	2 (2%)

Table 3. *Cont.*

Category (Characteristic)	Description	Cases, *n* (%)
Maximum Size	<3 mm	30 (25%)
	3 to <15 mm	56 (46%)
	15 to <25 mm	20 (16%)
	≥25 mm	16 (13%)
Location	Internal carotid artery	60 (49%)
	Middle cerebral artery	32 (26%)
	Anterior cerebral artery	8 (7%)
	Posterior cerebral artery	3 (2%)
	Basilar artery	12 (10%)
	Other	7 (6%)
Shape	Saccular	36 (30%)
	Non-saccular	86 (70%)
Position	Lateral	69 (57%)
	Bifurcation	32 (26%)
	Unclassifiable	21 (17%)
Type	Blister-like	39 (32%)
	Fusiform	8 (7%)
	Eccentric-fusiform	9 (7%)
	Fusiform-saccular	9 (7%)
	Unclassifiable	57 (47%)

3.2. Image Acquisition

CTA data were acquired using CT scanners from six manufacturers: Toshiba IT & Control Systems Corporation (Tokyo, Japan; n = 128), Siemens Healthineers (Erlangen, Germany; n = 23), GE Healthcare (Chicago, IL, USA; n = 12), Philips Healthcare (Amsterdam, Netherlands; n = 7), Canon Medical Systems (Otawara, Japan; n = 1), and Hitachi, Ltd. (Tokyo, Japan; n = 1). Examinations were performed with a slice thickness of 0.5–2 mm and a matrix size of 512 × 512 pixels. All patients received an intravenous iodinated contrast agent at a weight-adjusted dose. All images covered the brain; however, in some cases several slices in the vertex region were missing. Some studies also include the neck. All images were stored in DICOM format, making them compatible with standard medical imaging software.

3.3. Data Depersonalization

All data were anonymized through the removal of any potentially identifying personal and institutional information. DICOM technical metadata were preserved.

In addition, to ensure full confidentiality, a defacing procedure was performed. We used an algorithm based on a publicly available pretrained model for automatic facial segmentation (CTA-DEFACE) [38]. The model detected the facial soft tissues (from the forehead to the chin) and generated 3D masks. The segmented region was then automatically refined using morphological operations. Morphological operations such as dilation, erosion, and hole filling were applied to smooth object boundaries, eliminate gaps in the mask caused by segmentation errors, and remove noise components unrelated to the facial region. After preprocessing, the frontal portion of each image corresponding to the masks was removed. This approach ensured complete anonymization of the studies without affecting intracranial structures.

3.4. Intracranial Aneurysm Segmentation

Intracranial aneurysms were segmented by two experienced clinicians: a neuroradiologist and a neurosurgeon. The IA-positive cases were randomly divided into two equal subsets, with each expert independently performing segmentations on one subset using the radiology workstation "Gamma Multivox D2" (Gammamed-Soft, Ltd., Moscow, Russia).

After defining the region of interest on the three-dimensional reconstruction, segmentation was performed using intensity thresholding, with the threshold values determined by the expert individually for each study to optimally capture the aneurysm volume (Figure 2).

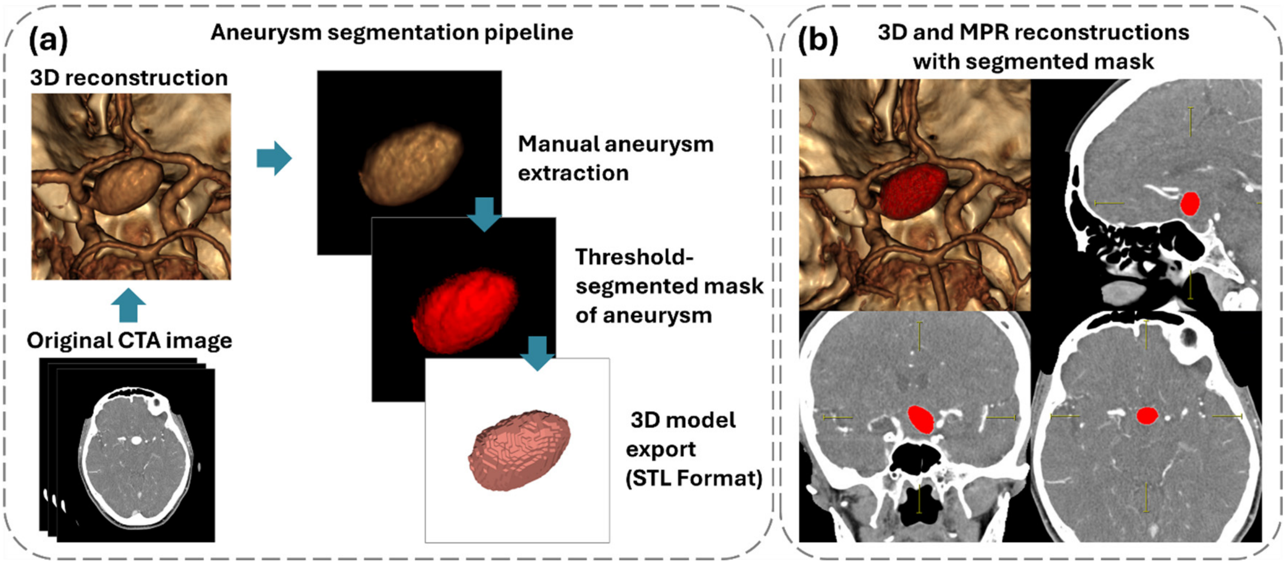

Figure 2. Annotation workflow for cerebral aneurysms: (**a**) segmentation pipeline; (**b**) multiplanar visualization with segmented aneurysm highlighting (red).

The segmented object represented only the aneurysm sac (lumen) without arteries uninvolved by the pathology. The extracted object included only the contrast-opacified blood volume and excluded the thrombosed and calcified portions of the aneurysms.

Both experts then reviewed the annotations of the counterpart. In the event of any discrepancies, the case was discussed jointly, and a consensus was reached to generate the final segmentation. The finalized segmentations were exported as a polygonal surface in STL format.

3.5. Aneurysm Classification

This subsection details the clinical and image-based criteria that form the basis for the aneurysm classification and morphometric data compiled in the metadata file (Metadata.csv). The structure of this file is described in Section 2.2. These metadata enable efficient, targeted filtering of cases for specific research needs.

By morphology, IAs were classified as saccular or non-saccular; the aneurysm's location relative to the parent vessel was noted (lateral, bifurcation, or unclassifiable within this scheme), and an expanded classification of non-saccular aneurysms by type was also provided (Figure 3).

To facilitate querying the dataset for specific lesion morphologies, non-saccular aneurysms were classified into blister-like, fusiform, eccentric-fusiform, and fusiform–saccular types. Blister-like aneurysms appear hemispheric, with the base representing the widest portion of the dome. Fusiform aneurysms are defined as a uniform, spindle-shaped dilatation of a vessel segment, whereas eccentric-fusiform aneurysms are characterized by an offset relative to the vessel's central axis. Finally, aneurysms with complex morphology, combining dilatation of the parent vessel, branching vessels, and a dome-like outpouching were designated as fusiform–saccular. If a case could not be assigned to any class, it was labeled "Unclassifiable." Examples from this dataset for each category are shown in Figure 3.

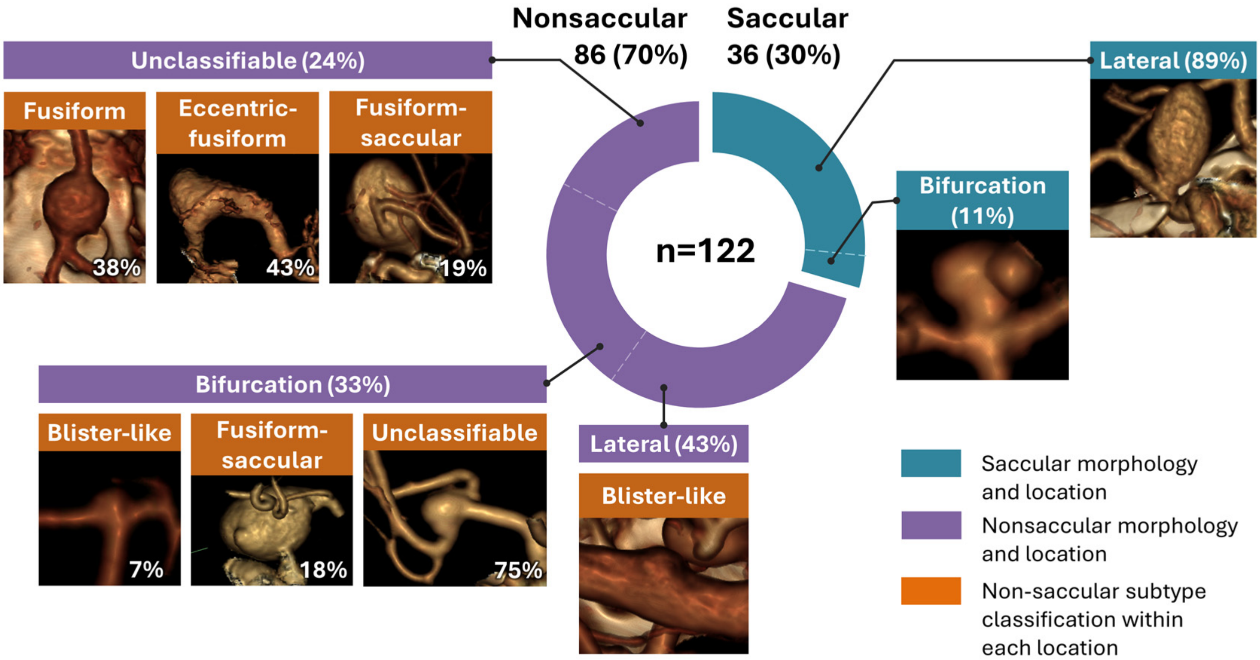

Figure 3. Classificational composition of the aneurysm dataset: hierarchical distribution with relative proportions. Percentages represent proportions relative to immediate parent category.

Morphological parameters were measured and recorded to enable more refined data selection during use. All linear measurements were performed manually by an experienced radiologist at a workstation using multiplanar reconstruction of the original axial slices. To improve measurement accuracy, standard tools were used to adjust image display (window width/window level), reorient section planes, and modify slice thickness. For fusiform aneurysms, maximum length was defined as the distance from the beginning to the end of the dilatation; in all other cases, maximum length was defined as the distance from the center of the neck base to the most remote point on the dome. Maximum width was defined as the largest transverse diameter of the aneurysm dome. Aneurysm neck width, when present, was also recorded (Figure 4a).

For bifurcation aneurysms with a well-defined neck and an unaltered size of the parent-artery bifurcation, the neck width and the maximum dome length measured from the neck were recorded. When the arterial bifurcation itself was involved in the pathological process, maximum length was measured from the onset of the dilatation, and the neck was considered absent. The reported aneurysm volume was computed on the already segmented object. Based on the maximum measured dimension, aneurysms were categorized by size as miliary (<3 mm), medium (3–15 mm), large (15–25 mm), and giant (>25 mm) (Figure 4b).

In collaboration with a neurosurgeon, we identified and recorded the key aneurysm morphological features that complicate surgical management: the presence of vessels arising from the aneurysm dome, mural thrombosis and wall calcification, and the presence of additional bulges (bleb) on the dome.

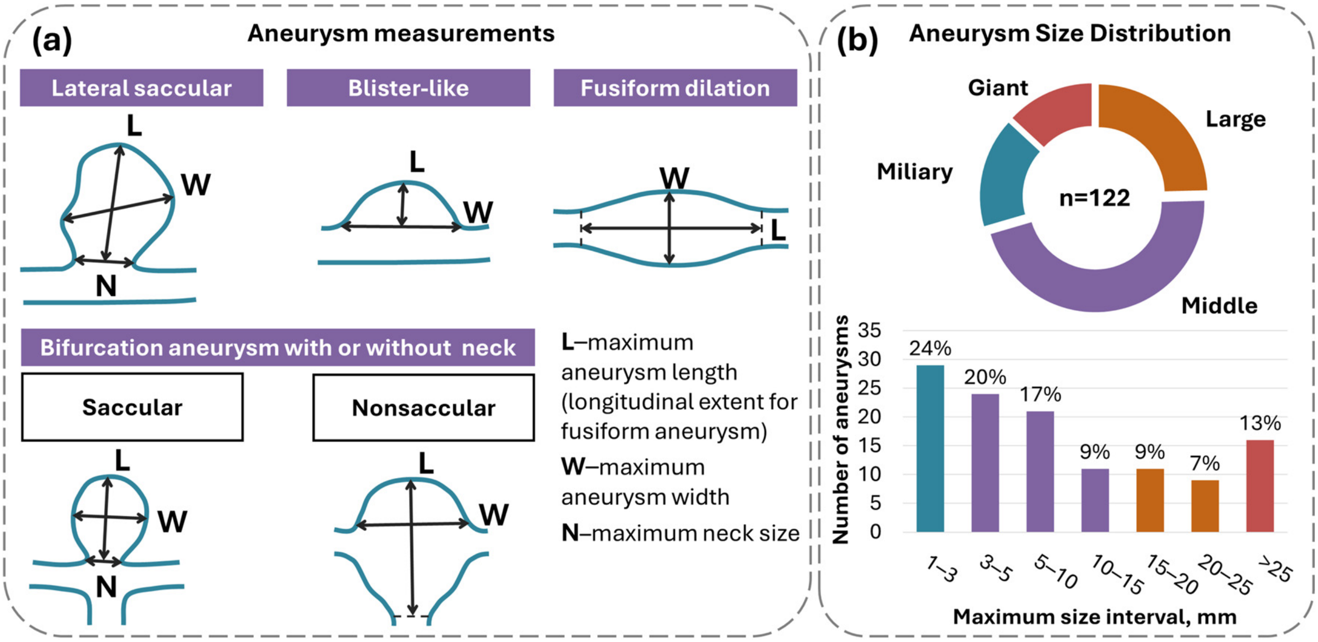

Figure 4. Aneurysm sizing: measurement guidelines for different morphological variants (**a**) and cohort distribution (**b**).

3.6. Quality Assurance and Technical Validation

All CTA scans were acquired as part of routine clinical workflows using imaging protocols approved by the respective institutions. All CT scanners used undergo regular maintenance and calibration. The segmentation process included cross validation of the segmented objects by two experienced clinicians and joint discussion in case of any discrepancies. This procedure ensured that the final annotations reflect a validated, agreed-upon ground truth. The experts also validated defacing across all series.

4. Usage Notes

The dataset is publicly available in the Zenodo repository at https://doi.org/10.5281/zenodo.15697196 [37], under the Creative Commons Attribution 4.0 International license (CC BY 4.0). The dataset files may be used without restriction provided that this publication is appropriately cited in any resulting work.

All STL, CSV, and DICOM files were verified for compatibility with multiple medical imaging and visualization software platforms.

Author Contributions: Conceptualization, A.G. and V.K.; methodology, D.D., E.B. and N.P.; software, D.P.; validation, N.P. and E.B.; investigation, E.G. and N.P.; resources, E.G., N.P. and V.K.; data curation, E.G., N.P. and E.B.; writing—original draft preparation, E.B. and N.P.; writing—review and editing, A.G., D.D. and V.K.; visualization, E.B.; supervision, A.G.; project administration, A.G. and V.K. All authors have read and agreed to the published version of the manuscript.

Funding: This research received no external funding.

Institutional Review Board Statement: The study was conducted in accordance with the Declaration of Helsinki, and approved by the Biomedical Ethics Committee of the N.V. Sklifosovsky Research Institute for Emergency Medicine (Protocol code. 2-23 dated 28 March 2023).

Informed Consent Statement: Patient consent was waived due to the institutions' provision of access to pre-anonymized retrospective data.

Data Availability Statement: The original data presented in the study are openly available in the Zenodo repository at https://doi.org/10.5281/zenodo.15697196 [37].

Conflicts of Interest: Evgenia Blagosklonova and Denis Pakhomov are full-time employees of Gammamed-Soft, Ltd. Andrey Gavrilov and Daria Dolotova are part-time employees of Gammamed-Soft, Ltd. Gammamed-Soft, Ltd. develops the Gamma-Multivox radiology workstation, which was used in this study for the analysis and annotation of CTA images. The company had no role in the study design, data interpretation, or the conclusions of the study.

Abbreviations

The following abbreviations are used in this manuscript:

3D	Three-dimensional
DICOM	Digital Imaging and Communications in Medicine
CT	Computed Tomography
CTA	Computed Tomography Angiography
IA	Intracranial Aneurysm
DSA	Digital Subtraction Angiography
MRA	Magnetic Resonance Angiography
TOF-MRA	Time-Of-Flight Magnetic Resonance Angiography
3DRA	3D Rotational Angiography
CADA	Cerebral Aneurysm Detection and Analysis challenge
ADAM	Aneurysm Detection and segMentation challenge
PHASES	(Population, Hypertension, Age, Size, Earlier Sah, Site) Risk Prediction Score
UIATS	Unruptured Intracranial Aneurysm Treatment Score

References

1. Etminan, N.; Chang, H.-S.; Hackenberg, K.; de Rooij, N.K.; Vergouwen, M.D.I.; Rinkel, G.J.E.; Algra, A. Worldwide Incidence of Aneurysmal Subarachnoid Hemorrhage According to Region, Time Period, Blood Pressure, and Smoking Prevalence in the Population. *JAMA Neurol.* **2019**, *76*, 588–597. [CrossRef] [PubMed]
2. Lawton, M.T.; Vates, G.E. Subarachnoid Hemorrhage. *N. Engl. J. Med.* **2017**, *377*, 257–266. [CrossRef] [PubMed]
3. van Gijn, J.; Kerr, R.S.; Rinkel, G.J. Subarachnoid Haemorrhage. *Lancet* **2007**, *369*, 306–318. [CrossRef] [PubMed]
4. Toth, G.; Cerejo, R. Intracranial Aneurysms: Review of Current Science and Management. *Vasc. Med.* **2018**, *23*, 276–288. [CrossRef]
5. Moawad, A.W.; Fuentes, D.T.; ElBanan, M.G.; Shalaby, A.S.; Guccione, J.; Kamel, S.; Jensen, C.T.; Elsayes, K.M. Artificial Intelligence in Diagnostic Radiology: Where Do We Stand, Challenges, and Opportunities. *J. Comput. Assist. Tomogr.* **2022**, *46*, 78–90. [CrossRef]
6. Feng, J.; Zeng, R.; Geng, Y.; Chen, Q.; Zheng, Q.; Yu, F.; Deng, T.; Lv, L.; Li, C.; Xue, B.; et al. Automatic Differentiation of Ruptured and Unruptured Intracranial Aneurysms on Computed Tomography Angiography Based on Deep Learning and Radiomics. *Insights Imaging* **2023**, *14*, 76. [CrossRef]
7. Xie, Y.; Liu, S.; Lin, H.; Wu, M.; Shi, F.; Pan, F.; Zhang, L.; Song, B. Automatic Risk Prediction of Intracranial Aneurysm on CTA Image with Convolutional Neural Networks and Radiomics Analysis. *Front. Neurol.* **2023**, *14*, 1126949. [CrossRef]
8. Liu, X.; Mao, J.; Sun, N.; Yu, X.; Chai, L.; Tian, Y.; Wang, J.; Liang, J.; Tao, H.; Yuan, L.; et al. Deep Learning for Detection of Intracranial Aneurysms from Computed Tomography Angiography Images. *J. Digit. Imaging* **2022**, *36*, 114–123. [CrossRef]
9. Meng, C.; Yang, D.; Chen, D. Cerebral Aneurysm Image Segmentation Based on Multi-Modal Convolutional Neural Network. *Comput. Methods Programs Biomed.* **2021**, *208*, 106285. [CrossRef]
10. Yang, J.; Xie, M.; Hu, C.; Alwalid, O.; Xu, Y.; Liu, J.; Jin, T.; Li, C.; Tu, D.; Liu, X.; et al. Deep Learning for Detecting Cerebral Aneurysms with CT Angiography. *Radiology* **2021**, *298*, 155–163. [CrossRef]
11. Shahzad, R.; Pennig, L.; Goertz, L.; Thiele, F.; Kabbasch, C.; Schlamann, M.; Krischek, B.; Maintz, D.; Perkuhn, M.; Borggrefe, J. Fully Automated Detection and Segmentation of Intracranial Aneurysms in Subarachnoid Hemorrhage on CTA Using Deep Learning. *Sci. Rep.* **2020**, *10*, 21799. [CrossRef] [PubMed]
12. Park, A.; Chute, C.; Rajpurkar, P.; Lou, J.; Ball, R.L.; Shpanskaya, K.; Jabarkheel, R.; Kim, L.H.; McKenna, E.; Tseng, J.; et al. Deep Learning–Assisted Diagnosis of Cerebral Aneurysms Using the HeadXNet Model. *JAMA Netw. Open* **2019**, *2*, e195600. [CrossRef] [PubMed]
13. Din, M.; Agarwal, S.; Grzeda, M.; Wood, D.A.; Modat, M.; Booth, T.C. Detection of Cerebral Aneurysms Using Artificial Intelligence: A Systematic Review and Meta-Analysis. *J. Neurointerv. Surg.* **2023**, *15*, 262–271. [CrossRef] [PubMed]

14. Greving, J.P.; Wermer, M.J.H.; Brown, R.D.; Morita, A.; Juvela, S.; Yonekura, M.; Ishibashi, T.; Torner, J.C.; Nakayama, T.; Rinkel, G.J.E.; et al. Development of the PHASES Score for Prediction of Risk of Rupture of Intracranial Aneurysms: A Pooled Analysis of Six Prospective Cohort Studies. *Lancet Neurol.* **2014**, *13*, 59–66. [CrossRef]
15. Etminan, N.; Brown, R.D.; Beseoglu, K.; Juvela, S.; Raymond, J.; Morita, A.; Torner, J.C.; Derdeyn, C.P.; Raabe, A.; Mocco, J.; et al. The Unruptured Intracranial Aneurysm Treatment Score. *Neurology* **2015**, *85*, 881–889. [CrossRef]
16. Neulen, A.; Pantel, T.; König, J.; Brockmann, M.A.; Ringel, F.; Kantelhardt, S.R. Comparison of Unruptured Intracranial Aneurysm Treatment Score and PHASES Score in Subarachnoid Hemorrhage Patients With Multiple Intracranial Aneurysms. *Front. Neurol.* **2021**, *12*, 616497. [CrossRef]
17. Juchler, N.; Schilling, S.; Bijlenga, P.; Kurtcuoglu, V.; Hirsch, S. Shape Trumps Size: Image-Based Morphological Analysis Reveals That the 3D Shape Discriminates Intracranial Aneurysm Disease Status Better Than Aneurysm Size. *Front. Neurol.* **2022**, *13*, 809391. [CrossRef]
18. Lipp, S.N.; Niedert, E.E.; Cebull, H.L.; Diorio, T.C.; Ma, J.L.; Rothenberger, S.M.; Stevens Boster, K.A.; Goergen, C.J. Computational Hemodynamic Modeling of Arterial Aneurysms: A Mini-Review. *Front. Physiol.* **2020**, *11*, 454. [CrossRef]
19. de Nys, C.M.; Liang, E.S.; Prior, M.; Woodruff, M.A.; Novak, J.I.; Murphy, A.R.; Li, Z.; Winter, C.D.; Allenby, M.C. Time-of-Flight MRA of Intracranial Aneurysms with Interval Surveillance, Clinical Segmentation and Annotations. *Sci. Data* **2024**, *11*, 555. [CrossRef]
20. Di Noto, T.; Marie, G.; Tourbier, S.; Alemán-Gómez, Y.; Esteban, O.; Saliou, G.; Bach Cuadra, M.; Hagmann, P.; Richiardi, J. Lausanne_TOF-MRA_Aneurysm_Cohort. *OpenNeuro* **2022**. [CrossRef]
21. Ivantsits, M.; Goubergrits, L.; Kuhnigk, J.-M.; Huellebrand, M.; Brüning, J.; Kossen, T.; Pfahringer, B.; Schaller, J.; Spuler, A.; Kuehne, T.; et al. Cerebral Aneurysm Detection and Analysis Challenge 2020 (CADA). In *Proceedings of the Cerebral Aneurysm Detection and Analysis. CADA 2020. Lecture Notes in Computer Science(R0), vol 12643*; Hennemuth, A., Goubergrits, L., Ivantsits, M., Kuhnigk, J., Eds.; Springer: Cham, Switzerland, 2021; pp. 3–17.
22. Aneurysm Detection And segMentation Challenge (ADAM). Available online: http://adam.isi.uu.nl/ (accessed on 15 January 2026).
23. Juchler, N.; Bijlenga, P.; Hirsch, S. AneuX Morphology Database. *Zenodo* **2022**. [CrossRef]
24. Benkner, S.; Arbona, A.; Berti, G.; Chiarini, A.; Dunlop, R.; Engelbrecht, G.; Frangi, A.F.; Friedrich, C.M.; Hanser, S.; Hasselmeyer, P.; et al. @neurIST: Infrastructure for Advanced Disease Management Through Integration of Heterogeneous Data, Computing, and Complex Processing Services. *IEEE Trans. Inf. Technol. Biomed.* **2010**, *14*, 1365–1377. [CrossRef] [PubMed]
25. Emory University, Department of Mathematics & Computer Science. AneuriskWeb Project Website. Available online: http://ecm2.mathcs.emory.edu/aneuriskweb (accessed on 20 March 2026).
26. Yang, X.; Xia, D.; Kin, T.; Igarashi, T. IntrA: 3D Intracranial Aneurysm Dataset for Deep Learning. In Proceedings of the 2020 IEEE/CVF Conference on Computer Vision and Pattern Recognition (CVPR), Seattle, WA, USA, 13–19 June 2020. [CrossRef]
27. Pozo Soler, J.; Frangi, A.F. Database of Cerebral Artery Geometries Including Aneurysms at the Middle Cerebral Artery Bifurcation. *Univ. Sheff.* **2017**. [CrossRef]
28. Westerlaan, H.E.; van Dijk, J.M.C.; Jansen-van der Weide, M.C.; de Groot, J.C.; Groen, R.J.M.; Mooij, J.J.A.; Oudkerk, M. Intracranial Aneurysms in Patients with Subarachnoid Hemorrhage: CT Angiography as a Primary Examination Tool for Diagnosis—Systematic Review and Meta-Analysis. *Radiology* **2011**, *258*, 134–145. [CrossRef]
29. Bo, Z.-H. Large IA Segmentation Dataset. *Zenodo* **2021**. [CrossRef]
30. Song, M.; Wang, S.; Qian, Q.; Zhou, Y.; Luo, Y.; Gong, X. Intracranial Aneurysm CTA Images and 3D Models Dataset with Clinical Morphological and Hemodynamic Data. *Sci. Data* **2024**, *11*, 1213. [CrossRef]
31. Barletta, E.; Gaspar, R.M.L.; Araújo, J.M.; Neves, M.F.; de Aquino, J.B.; Belsuzarri, T.B. Nonsaccular Aneurysms: A Wide Comparison between the Four Main Types. *Surg. Neurol. Int.* **2019**, *10*, 30. [CrossRef]
32. Papasilekas, T.I.; Themistoklis, K.M.; Korfias, S.I.; Sakas, D.E. Blister Aneurysms. In *Vascular Malformations of the Central Nervous System*; IntechOpen: Rijeka, Croatia, 2020.
33. Diana, F.; Romoli, M.; Raz, E.; Agid, R.; Albuquerque, F.C.; Arthur, A.S.; Beck, J.; Berge, J.; Boogaarts, H.D.; Burkhardt, J.-K.; et al. Complex Intracranial Aneurysms: A DELPHI Study to Define Associated Characteristics. *Acta Neurochir.* **2024**, *166*, 294. [CrossRef]
34. Togashi, S.; Shimizu, H. Complex Intracranial Aneurysms. *Adv. Tech. Stand. Neurosurg.* **2022**, *44*, 225–238.
35. Bruneau, M.; Amin-Hanjani, S.; Koroknay-Pal, P.; Bijlenga, P.; Jahromi, B.R.; Lehto, H.; Kivisaari, R.; Schaller, K.; Charbel, F.; Khan, S.; et al. Surgical Clipping of Very Small Unruptured Intracranial Aneurysms: A Multicenter International Study. *Neurosurgery* **2016**, *78*, 47–52. [CrossRef]
36. Joseph, F.J.; Vanluchene, H.E.R.; Bervini, D. Simulation Training Approaches in Intracranial Aneurysm Surgery—A Systematic Review. *Neurosurg. Rev.* **2023**, *46*, 101. [CrossRef]
37. Blagosklonova, E.; Dolotova, D.; Polunina, N.; Grigorieva, E.; Pakhomov, D.; Krylov, V.; Gavrilov, A. Open Dataset of Annotated DICOM Images of Head CTA for Intracranial Aneurysm Detection. *Zenodo* **2025**. [CrossRef]

38. Mahmutoglu, M.A.; Rastogi, A.; Schell, M.; Foltyn-Dumitru, M.; Baumgartner, M.; Maier-Hein, K.H.; Deike-Hofmann, K.; Radbruch, A.; Bendszus, M.; Brugnara, G.; et al. Deep Learning-Based Defacing Tool for CT Angiography: CTA-DEFACE. *Eur. Radiol. Exp.* **2024**, *8*, 111. [CrossRef]